TESTING THE EQUIVALENCE PRINCIPLE IN AN EINSTEIN ELEVATOR:

DETECTOR DYNAMICS AND GRAVITY PERTURBATIONS

E.C. Lorenzini[1,*], I.I. Shapiro[1], M.L. Cosmo[1], J. Ashenberg[1], G. Parzianello[2], V. Iafolla[3] and S. Nozzoli[3]

[1]Harvard-Smithsonian Center for Astrophysics (CfA), Cambridge, Massachusetts;
[2]University of Padova (Padua, Italy) and CfA Visiting Student;
[3]Institute of Space Physics (Rome, Italy).
[*]Corresponding author e-mail: elorenzini@cfa.harvard.edu

Abstract

We discuss specific, recent advances in the analysis of an experiment to test the Equivalence Principle (EP) in free fall. A differential accelerometer detector with two proof masses of different materials free falls inside an evacuated capsule previously released from a stratospheric balloon. The detector spins slowly about its horizontal axis during the fall. An EP violation signal (if present) will manifest itself at the rotational frequency of the detector. The detector operates in a quiet environment as it slowly moves with respect to the co-moving capsule. There are, however, gravitational and dynamical noise contributions that need to be evaluated in order to define key requirements for this experiment. Specifically, higher-order mass moments of the capsule contribute errors to the differential acceleration output with components at the spin frequency which need to be minimized. The dynamics of the free falling detector (in its present design) has been simulated in order to estimate the tolerable errors at release which, in turn, define the release mechanism requirements. Moreover, the study of the higher-order mass moments for a worst-case position of the detector package relative to the cryostat has led to the definition of requirements on the shape and size of the proof masses.

Introduction

The scientific goal of the experiment is to test the equality of gravitational and inertial mass (i.e., to test the Principle of Equivalence) by measuring the independence of the rate of fall of bodies from their mass and composition. The experiment is accomplished by measuring the relative displacement (or equivalently acceleration) of two falling bodies of different materials which are the proof masses of a differential accelerometer. The experiment goal is to measure the Eötvös ratio $\Delta g/g$ (differential acceleration/common acceleration) with an accuracy about two orders of magnitude better than presently achieved[i,ii]. The experiment is a null experiment in which a relative displacement different from zero, at the spin frequency, between the proof masses will indicate a violation of the Equivalence Principle.

In summary, the experiment consists in taking differential acceleration measurements with a high-sensitivity detector (the sensor) during free fall conditions lasting up to 28 s in a disturbance-free acceleration environment. A capsule is first released from the balloon at an altitude of typically 40 km and the detector is released from the top of the capsule immediately afterwards. During the measurement phase, the sensor free falls inside a 2-meters-long (in the vertical direction) evacuated cryostat (contained inside the capsule) that is falling simultaneously in the rarefied atmosphere[iii].

By falling in vacuum inside a co-moving capsule, the noise acceleration level can be kept to a negligible level while the signal strength in free fall, i.e., the full-strength Earth's gravity, is increased by 3 orders of magnitude with respect to the signals available to EP experiments conducted on the ground. The free fall technique, therefore, combines some of the advantages of the space-based tests with the accessibility and reusability of ground experiments.

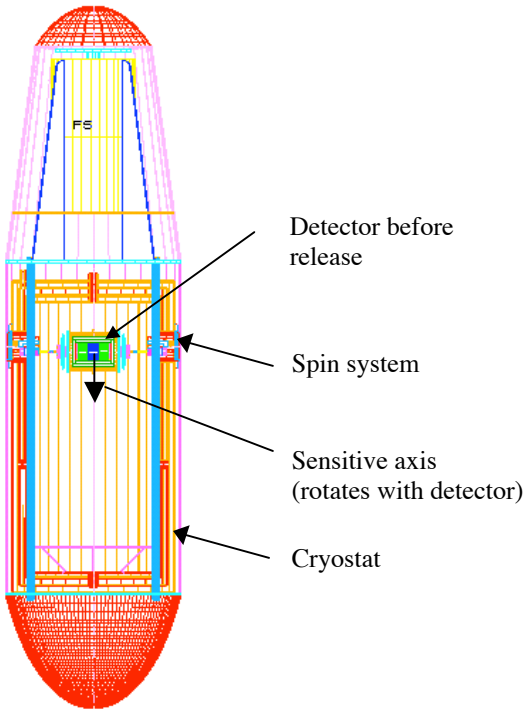

Figure 1 Schematic of capsule with detector attached (before release) to the spin up system

The detector has two sensing masses of different materials with their centers of mass (CM) as coincident as possible in order to reduce the effect of gravity gradients. The two masses are constrained in a way that they can move at low frequency along one axis (i.e., the sensitive axis that is perpendicular to the symmetry axis of the sensor) while they are rigidly constrained about the other two axes. The displacement of each sensing mass along the sensitive axis is detected by capacitive pickups which are parts of a measurement bridge.

One key feature is that the detector is spun before release about the symmetry axis that lies on the horizontal plane. The rotation provides the modulation (at the spin frequency) of any possible violation signal. Moreover, the spin provides gyroscopic stabilization of the detector during the fall and separates the signal from key noise components generated by the detector dynamics.

Frequency separation between the signal and the largest noise components is essential to the success of the experiment. The noise components that, unavoidably, appear at the signal frequency need to have a strength well below the detector threshold sensitivity. In the following, we analyze the detector dynamics to identify the frequencies of noise components that can be separated from the signal thanks to the appropriate selection of the inertia characteristics of the detector package. We also study the higher-order mass moments generated by the capsule mass and acting on the sensing masses. The higher-order mass moments contain some components at the signal frequency and care must be taken in designing the sensing masses in order to reduce the strength of those components to a negligible level.

Analysis of Higher-order Mass Moments

Overview

The sensing mass (test body), falling inside the capsule, is subjected to non-negligible gravitational attraction by the capsule. The higher-order gravitational potential plays a key role because of the elimination of the zero-order potential due to the Equivalence Principle. The model of perturbing gravitational mass consists of a spinning test body inside a capsule that is a hollow cylinder covered with flat caps. The test body is released at the symmetry axis of the cylinder, and deviates from the axis during its fall. Our goal is to compute the gravitational force and torque acting in the neighborhood of the fall trajectory. The fact that both the test mass and the capsule are closed finite bodies, increases the complexity of the problem. We are mostly concerned here with the harmonics of the force/torque at the modulation frequency as seen in the reference frame of the detector. In other words, our model should evaluate the force/torque in the rotating body frame of the sensing mass. For that purpose we built a semi-analytical model that can handle any configuration of test mass as well as any additional mass attached to the distributed mass of the capsule. Moreover, we exploited the fact that the size of the test mass is smaller than the cylinder radius to derive an asymptotic analytical solution.

There are at least three ways to approach the computation of the gravitational attraction between the capsule and the test body. The first approach is to compute the force between each capsule mass element and a test body mass element, and to perform a double summation on these forces. If N is the number of capsule mass elements, and N_B is the number of test body mass elements, then the cardinality of the computation (that drives the computational load) is $N \quad N_B$. As it will become apparent later on, the mass discretization resolution required to the test body is very demanding and, consequently, the cardinality becomes prohibitively high with this approach. The second approach is a double integration over the bodies. The drawback of the first approach is

the heavy computational effort, especially if the computation is needed as an online computation in a dynamical process. The weakness of the second approach is in the cumbersome analytical computation. The integration will require an asymptotic series expansion of complicated functions and asymptotic series introduce a truncation error into the computation. We adopted a third approach for the gravitational model.

We consider the capsule as a discrete ensemble of lumped mass, where the resultant force and torque acting on the test body are the cumulative force and torque due to the summation of all the capsule mass elements. The gravitational potential of the test body is expanded according to its increasing-order inertia characteristics. In other words, the interaction is between a finite body (the test mass) and a point mass. This approach is the result of a tradeoff between the previous approaches and its cardinality is N. The main advantage is the flexibility of modeling any capsule shape and the strongly reduced computational load.

The purpose of the following computation is to derive a closed-form analytical expressions, for the force and torque acting on the spinning test mass due to a capsule mass element.

Gravitational Model

The gravitational potential between finite size bodies, is:

$$V = -G \int_{o} \int_{B} \frac{dM_B}{r} dM_o \qquad (1)$$

where $_B$ is the test body (proof mass), and $_0$ represents the attracting bodies, namely, the capsule or any other perturbing body.

For the purpose of simplicity we will proceed with a formulation of the test body and a single element of the attracting mass, M_i.

The gravitational potential at a representative element mass M_i due to the test body is: $V(M_i) = -GM_i \int_{M_B} \frac{dM_B}{r}$, where $\vec{r}$ is the radius vector between a mass element of the test body and dM_o as shown in Fig. 2.

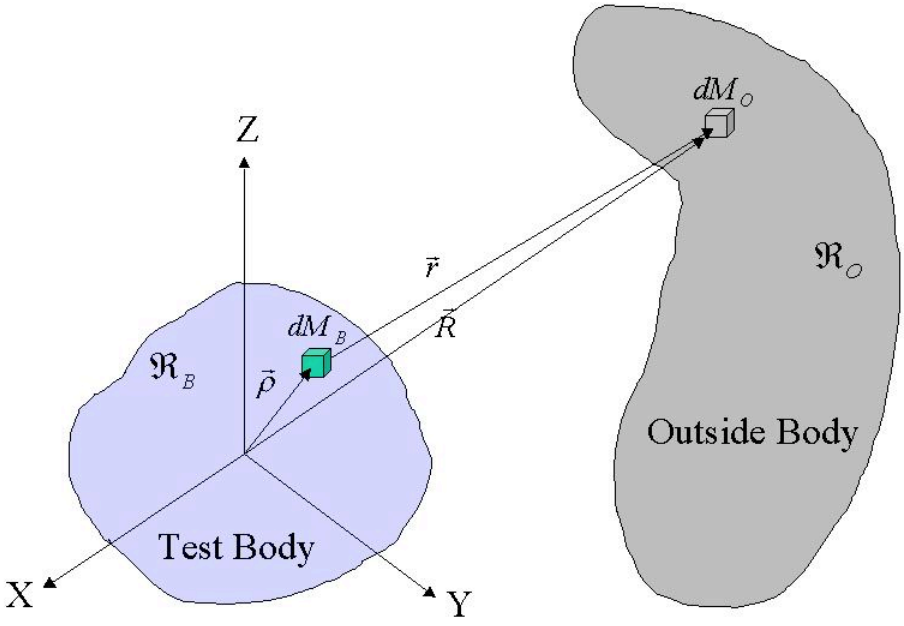

Figure 2 Gravitation model for test mass and outer attracting bodies

Assuming a sufficient discretization, the total force acting on the test body due to all external mass elements is $\vec{F}_B = \sum_{i=1}^{N} V(M_i)$, where N is the number of external mass elements. We first erect the following reference frames. The capsule frame, denoted by $\{X, Y, Z\}$ is attached to the capsule. X, Y lie on the equatorial plane and have an arbitrary azimuth while Z coincides with the symmetry axis of the capsule/cylinder. The test body frame, denoted by $\{x, y, z\}$, is attached to the test mass. The gravitational potential will be expressed in body frame. The inertia coefficients of the body are constant in this frame.

The derivation consists of the following steps: (1) substituting the inverse radius approximation into the potential; and (2) carrying out the integration. The position vectors in body frame are as follows:

$$\vec{R} = (l\,e_x + m\,e_y + n\,e_z)\,R \quad \text{and} \quad \vec{\rho} = x\,e_x + y\,e_y + z\,e_z$$

where $\{e_x, e_y, e_z\}$ are body unit vectors, and $\{l, m, n\}$ are direction cosines between $\vec{R}$ and the body axes.

The resulting potential is a summation over all mass elements M_i (only the first 4 terms are shown for the sake of brevity):

$$
\begin{aligned}
V = \sum_{i=1}^{N} \{ & -\frac{GM_1M_2}{R} - \frac{GM_1M_2}{R^2}\left[l\bar{x} + m\bar{y} + n\bar{z}\right] \\
& - \frac{GM_1}{2R^3}[(3l^2 - 1)J_{xx} + (3m^2 - 1)J_{yy} + (3n^2 - 1)J_{zz} + \\
& \qquad 6(lmJ_{xy} + lnJ_{xz} + mnJ_{yz})] \\
& - \frac{GM_1}{2R^4}[l(5l^2 - 3)J_{xxx} + m(5m^2 - 3)\,J_{yyy} + n(5n^2 - 3)J_{zzz} \\
& + 3m(5l^2 - 1)J_{xxy} + 3n(5l^2 - 1)\,J_{xxz} + 3l(5m^2 - 1)\,J_{xyy} \\
& + 3n(5m^2 - 1)\,J_{yyz} + 3l(5n^2 - 1)J_{xzz} + 3m(5n^2 - 1)J_{yzz} \\
& + 6lmnJ_{xyz}] + \Box(\frac{1}{R^5})\}
\end{aligned}
\tag{2}
$$

where $j_{x^p y^q z^r}$ are the inertia integrals defined as:

$$
j_{x^p y^q z^r} = \int_{M_B} x^p y^q z^r \, dm \tag{3}
$$

Expressions for the forces (shown in the following) are obtained by derivation of the potential. Torques (not shown here) are obtained by integrating over the proof mass the torque acting on a mass element of the body.

$$
\begin{aligned}
F_x = G \sum_{i=1}^{N} M_i \{ & \frac{M_B l}{R_i^2} + \frac{M_B}{R_i^3}\left[(3l_i^2 - 1)\bar{x} + 3l_i m_i \bar{y} + 3l_i n_i \bar{z}\right] \\
& + \frac{1}{R_i^4}[(\frac{5}{2}\Box_i - I_{yy} - I_{zz} + 2I_{xx})l_i + 3m_i(5l_i^2 - 1)I_{xy} + 3n_i(5l_i^2 - 1)I_{xz} + 15l_i m_i n_i I_{yz}] \\
& + \frac{1}{R_i^5}[\frac{1}{2}(35l_i^4 - 30l_i^2 + 3)J_{xxx} + \frac{5}{2}(7m_i^2 - 3)l_i m_i J_{yyy} + \frac{5}{2}(7n_i^2 - 3)l_i n_i J_{zzz} \\
& + \frac{15}{2}(7l_i^2 - 3)l_i m_i J_{xxy} + \frac{15}{2}(7l_i^2 - 3)l_i n_i J_{xxz} + \frac{3}{2}(35l_i^2 m_i^2 - 5l_i^2 - 5m_i^2 + 1)J_{xyy} \\
& + \frac{15}{2}(7m_i^2 - 1)l_i n_i J_{yyz} + \frac{3}{2}(35l_i^2 n_i^2 - 5l_i^2 - 5n_i^2 + 1)J_{xzz} + \frac{15}{2}(7n_i^2 - 1)l_i m_i J_{yzz} \\
& + 3(7l_i^2 - 1)m_i n_i J_{xyz}] + H.O.T\}
\end{aligned}
$$

$$
\begin{aligned}
F_y &= G\sum_{i=1}^{N} M_i\{\frac{M_B m_i}{R_i^2}+\frac{M_B}{R_i^3}\left[3l_i m_i\bar{x}+(3m_i^2-1)\bar{y}+3m_i n_i\bar{z}\right] \\
&+\frac{1}{R_i^4}[(\frac{5}{2}\Delta_i-\mathrm{I}_{xx}-\mathrm{I}_{zz}+2\mathrm{I}_{yy})m_i+3l_i(5m_i^2-1)\mathrm{I}_{xy}+15l_i m_i n_i\mathrm{I}_{xz}+3n_i(5m_i^2-1)\mathrm{I}_{yz}] \\
&+\frac{1}{R_i^5}[\frac{5}{2}(7l_i^2-3)l_i m_i\mathrm{J}_{xxx}+\frac{1}{2}(35m_i^4-30m_i^2+3)\mathrm{J}_{yyy}+\frac{5}{2}(7n_i^2-3)m_i n_i\mathrm{J}_{zzz} \\
&+\frac{3}{2}(35l_i^2m_i^2-5m_i^2-5l_i^2+1)\mathrm{J}_{xxy}+\frac{15}{2}(7l_i^2-1)m_i n_i\mathrm{J}_{xxz}+\frac{15}{2}(7m_i^2-3)l_i m_i\mathrm{J}_{xyy} \\
&+\frac{15}{2}(7m_i^2-3)m_i n_i\mathrm{J}_{yyz}+\frac{15}{2}(7n_i^2-1)l_i m_i\mathrm{J}_{xzz}+\frac{3}{2}(35m_i^2n_i^2-5m_i^2-5n_i^2+1)\mathrm{J}_{yzz} \\
&+3(7m_i^2-1)l_i n_i\mathrm{J}_{xyz}]+H.O.T\}
\end{aligned}
\tag{4}
$$

$$
\begin{aligned}
F_z &= G\sum_{i=1}^{N} M_i\{\frac{M_B l}{R_i^2}+\frac{M_B}{R_i^3}\left[3l_i n_i\bar{x}+3m_i n_i\bar{y}+3(n_i^2-1)\bar{z}\right] \\
&+\frac{1}{R_i^4}[(\frac{5}{2}\Delta_i-\mathrm{I}_{xx}-\mathrm{I}_{yy}+2\mathrm{I}_{zz})n_i+15l_i m_i n_i\mathrm{I}_{xy}+3l_i(5n_i^2-1)\mathrm{I}_{xz}+3m_i(5n_i^2-1)\mathrm{I}_{yz}] \\
&+\frac{1}{R_i^5}[\frac{5}{2}(7l_i^2-3)l_i n_i\mathrm{J}_{xxx}+\frac{5}{2}(7m_i^2-3)m_i n_i\mathrm{J}_{yyy}+\frac{1}{2}(35n_i^4-30n_i^2+3)\mathrm{J}_{zzz} \\
&+\frac{15}{2}(7l_i^2-1)m_i n_i\mathrm{J}_{xxy}+\frac{3}{2}(35l_i^2n_i^2-5l_i^2-5n_i^2+1)\mathrm{J}_{xxz}+\frac{15}{2}(7m_i^2-1)l_i n_i\mathrm{J}_{xyy} \\
&+\frac{3}{2}(35m_i^2n_i^2-5m_i^2-5n_i^2+1)\mathrm{J}_{yyz}+\frac{15}{2}(7n_i^2-1)l_i n_i\mathrm{J}_{xzz}+\frac{15}{2}(7n_i^2-3)m_i n_i\mathrm{J}_{yzz} \\
&+3(7n_i^2-1)l_i m_i\mathrm{J}_{xyz}]+H.O.T\}
\end{aligned}
$$

where H.O.T stands for higher-order terms and

$$\Delta_i=(\mathrm{I}_{yy}+\mathrm{I}_{zz}-2\mathrm{I}_{xx})l_i^2+(\mathrm{I}_{xx}+\mathrm{I}_{zz}-2\mathrm{I}_{yy})m_i^2+(\mathrm{I}_{xx}+\mathrm{I}_{yy}-2\mathrm{I}_{zz})n_i^2$$

Note that the force has the following order of magnitude:

$$F \sim \sum_i G\frac{M_i M_B}{R_i^2}\{O(1)+O(\frac{\bar{\rho}}{R_i})+O(\frac{L_B^2}{R_i^2})+O(\frac{L_B^3}{R_i^3})+H.O.T\}$$

Where L_B is a characteristic length of the test body with $\frac{L_B}{R_i}<<1$, and $\frac{\bar{\rho}}{R_i}<<1$.

Minimizing the higher-order effects

The goal is to minimize the gravitational forces acting on the test mass. The force equations reveal that the dominant term is the term corresponding to the second-order inertia. The offset term (dipole) is equal to zero for a reference frame centered at the body CM (see also later on). The direct way to minimize the forces is to require equal second-order moments of inertia. Then, the residual forces are due to mass imperfections and to higher-order (and smaller strength) inertia integrals. The purpose of the following discussion is to explore the effect of each term for a spinning test body.

First, we evaluate the mixed-inertia terms due to an imperfection. We assume that the imperfection is due to a disturbance in mass and/or length. The nominal test body could be a perfect cylinder, with radius R_B and length L_B. In order to minimize the force we require that $I_{XX} = I_{YY} = I_{ZZ}$. This constraint translates into a given aspect ratio of the cylinder as follows: $L_B = \sqrt{3} R_B$. Given the mass density, the mass or the size of the cylinder are now functions of a single free parameter. For example, given the mass, M_B, and the density, ρ_B, the length is: $L_B = \left(\frac{3 M_B}{\pi \rho_B} \right)^{\frac{1}{3}}$

The similarity dimension of the k-order inertia is $[I] = \left[ML^k \right]$. Thus, the perturbed k-order inertia is $\delta I = L^k \delta M + k M L^{k-1} \delta L$, or

$$\frac{\delta I}{I} = \frac{\delta M}{M} + k \frac{\delta L}{L}$$

Next, we consider the effect of the spin. The test body is spinning about its x-axis with a frequency that will be regarded as a fundamental frequency, or P1 (period one). We are primarily concerned with P1 because it is the frequency of the measured signal. For this purpose, we will analyze F_y by substituting the direction cosines, shown below, into the force expression.

The periodicity in time is introduced through the direction cosines that represent the orientation of the body frame relative to the capsule frame. The transformation between the two is:

$$\begin{bmatrix} x \\ y \\ z \end{bmatrix} = \begin{bmatrix} 1 & 0 & 0 \\ 0 & c\theta & s\theta \\ 0 & -s\theta & c\theta \end{bmatrix} \begin{bmatrix} X \\ Y \\ Z \end{bmatrix} \qquad (5)$$

The resulting direction cosines are:

$$l = \frac{x}{R} = \frac{X}{R} \ (independent \ \ of \ \ \theta)$$

$$m = \frac{y}{R} = \frac{Y c\theta + Z s\theta}{R} \qquad (6)$$

$$n = \frac{z}{R} = \frac{-Y s\theta + Z c\theta}{R}$$

l becomes a cyclic function only if the body deviates from the X-axis.

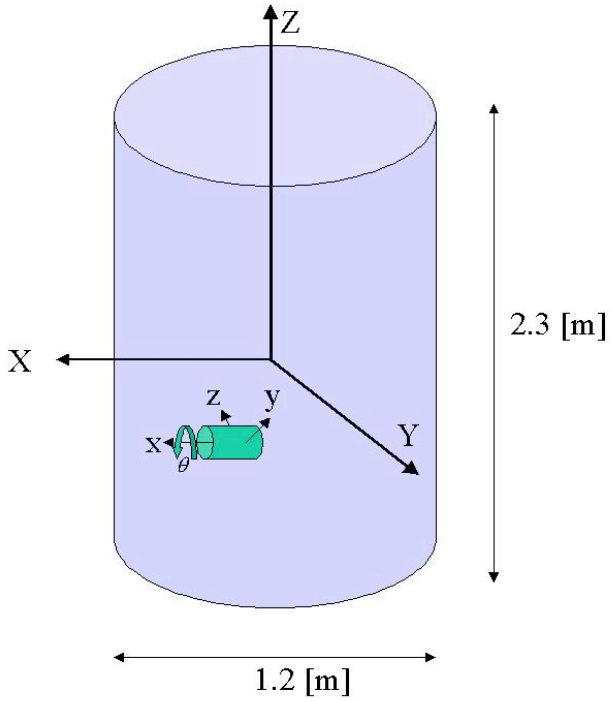

Figure 3 Reference frames

We compute the forces and torques acting on an imperfect proof mass placed at the worst location expected inside the capsule for conservative value of the wind shear (that is a point at –0.5 m below the capsule equator and 0.1 m off the centerline. The capsule consists of a hollow cylinder, covered by two flat caps with a total mass of 500 kg. The test body mass is 1 kg with sizes: $R_B = 0.0412 m$ and $L_B = 0.0713 m$. The geometrical and mass inhomogeneity errors, based on realistic assumptions, are: $\Delta L/L = 10^{-4}$ and $\Delta M/M = 10^{-4}$.

In the following plots (Figs. 4 and 5) we also show non-zero dipole terms (first-order inertia) to represent the fact the CM of one proof mass does not coincide with the CM of the other, thereby originating a non-null (gravity gradient) term when the difference of accelerations is taken between the two proof masses.

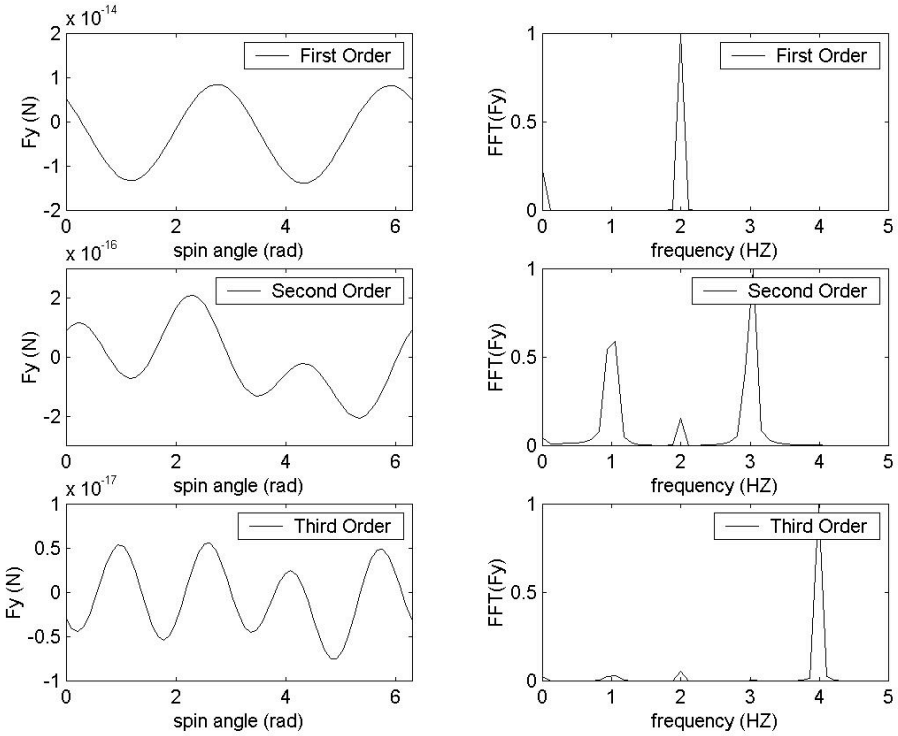

Figure 4 Ordered forces and spectra at expected worst location within the capsule

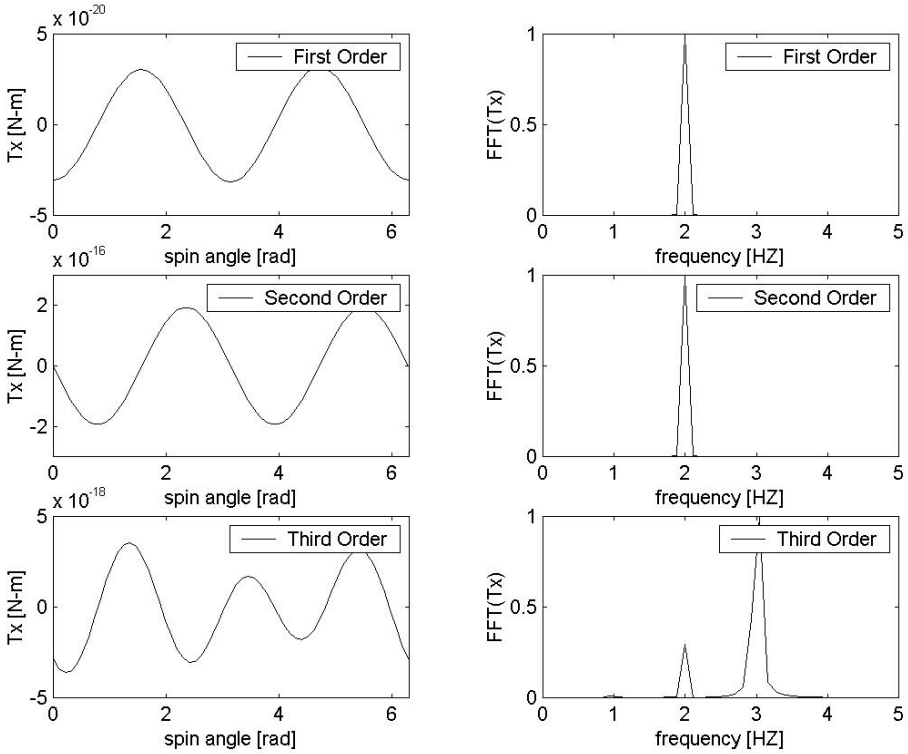

Figure 5 Ordered torques and spectra at expected worst location within the capsule

Similarity analysis

Another important issue is the role played by the test body mass and size. For this purpose we perform a similarity analysis, as shown in the following. We have formulated the gravitational potential as an asymptotic series in $1/R^n$. Each term in the series has an inertial tensor of degree $n - 1$. For example, the first term is of order n = 1 and its inertia tensor is of order 0 (the test body mass). The third term is of degree n = 3 and its inertia tensor is of order 2. This non-uniformity, however, introduces a problem when one computes the forces for a particular test mass and wants to deduct the forces for a different size of test mass. Mathematically speaking, if $F(M_{B1})$ and $F(M_{B2})$ are the forces due to two different test masses, then the ratio between the forces is not a homogeneous function, that is, $F(M_{B1})/F(M_{B2}) \neq g((M_{B1}/M_{B2})^m)$ where g is a function and m is the degree of the homogeneity. Note however that each term of the series is homogeneous by itself. For example, the first term is homogeneous of degree one, that is, the ratio between forces equals the ratio between the masses.

We will distinguish between two situations. The first situation is when the difference in masses is due to a different density. Since the forces are homogeneous of degree one in density, the ratio between the forces is equal to the ratio between the masses and the acceleration is constant. In a more interesting situation the density is the same, and the different mass is due to different sizes. In this case we need to apply a different similarity to each term. Let L and M be scaling factors for the length and the mass, respectively. If the density of different test bodies is the same, then $L \quad M^{1/3}$. Let $m = n - 1$ be the order of the moment of inertia, then its similarity dimension is $L^m M$, that is, $M^{1+m/3}$ or L^{m+3}. The acceleration similarity is $M^{m/3}$ or L^m. The following table summarizes the similarity dimension for each term in the potential.

Table 1 Similarity relations for the gravitational potential term

Potential Order $n; 1/R^n$	Inertia Order $m = n - 1$	Inertia Similarity	Acceleration Similarity
1	0	$M \quad (L^3)$	$1 \quad (1)$
2	1	$M^{4/3} \quad (L^4)$	$M^{1/3} \quad (L)$
3	2	$M^{5/3} \quad (L^5)$	$M^{2/3} \quad (L^2)$
4	3	$M^2 \quad (L^6)$	$M \quad (L^3)$
5	4	$M^{7/3} \quad (L^7)$	$M^{4/3} \quad (L^4)$

To summarize, given the force (or the acceleration) on a particular test body, we can deduct the force (acceleration) on another geometrically-scaled test mass. The acceleration ratio (of two different test masses with the same density) versus similarity dimensions (i.e., mass and length) is illustrated in Fig. 5.

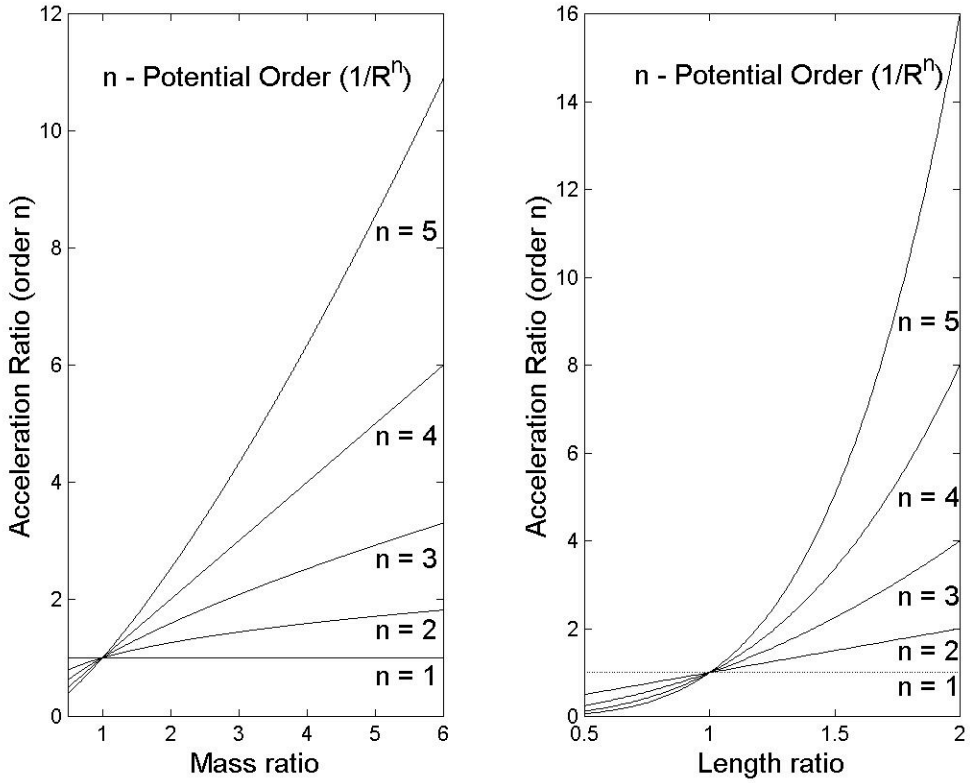

Figure 6 Scaling of test mass acceleration for masses with same density

The maximum potential order considered in our analysis is the hexadecapole (n = 5) which involves the fourth-order inertia integrals. We computed numerically the forces associated with the hexadecapole for a body with equal second-order inertia integrals (in order to minimize the quadrupole term). The results show that, at the worst expected location inside the capsule, the maximum acceleration associated with the hexadecapole term for a 1-kg proof mass is less than 10^{-16} g. In other words, for the accuracy goal of this experiment there is no need for belted cylinders[iv] (which would reduce the hexadecapole component even further). Proof masses with equal second-order inertia integrals (or alternatively moments of inertia), construction accuracy of order ten microns, and sizes smaller than about 10 cm are sufficient to make the contributions of all the higher-order gravity terms negligible.

Detector Dynamics

The instrument package dynamics also affects the differential accelerometer output. We derive the differential equations of motion for the detector in free fall (without gravity perturbations for the time being) and carry out numerical integrations for cases of interest. Those cases are associated with non-null offset positions of the centers of mass of the proof masses with respect to the CM of the instrument package and initial rotational velocity errors orthogonal to the spin velocity in order to evaluate the influence of those parameters on the differential output of the accelerometer.

Equations of motion

The sensor in its current, preliminary design (see Fig. 7) is composed of two sensing masses (A and B) having the CMs as coincident as possible with the CM of the external case. One proof mass has a dumbbell shape, while the other is a hollow cylinder. These two masses are constrained to the case C by means of elastic springs and they can pivot about an axis that is parallel to the axis of symmetry of the sensor. The whole detector is spun about the symmetry axis x.

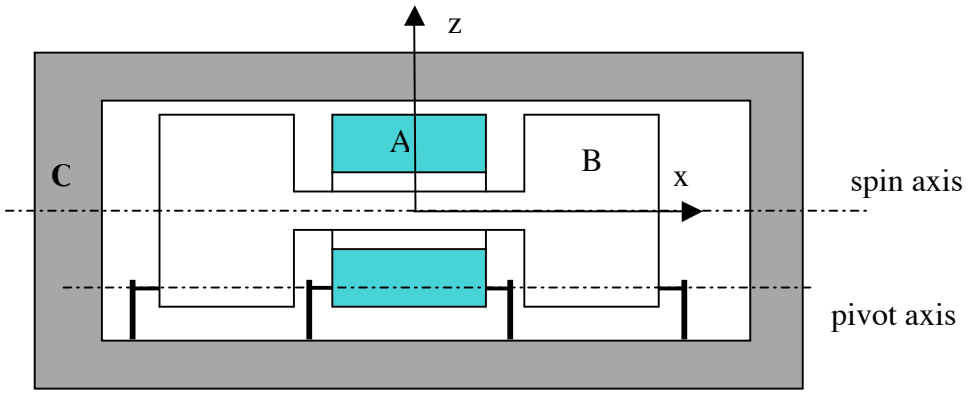

Figure 7 Schematic of three-body sensor

The motion of the sensor is essentially a rotation of the sensing masses about the pivot axis. The translational motion of the sensing masses, which depends on the high lateral stiffness of the springs is much smaller than the rotational motion. A rotation of the proof mass causes a variation of the distance between the sensing mass and the external case that changes the output capacitance.

Each body is modeled with six degrees of freedom, i.e., three translations and three rotations defined by Euler's angles. Elastic forces and torques are applied to each proof mass at the attachment points of the constraining springs. The transformation matrices have been written for each body in order to develop the equations of motion for the different bodies. The body coordinate systems are centered in the body's geometrical center, and are fixed with each body. The position of the CM is defined by three coordinates (x_{CMA}, y_{CMA}, z_{CMA} for body A) in the body reference frame. Each body frame has the x axis along the axis of symmetry which is also the spin axis. The y and z axes are radial axes that rotate with the body. The y axis is the sensitive axis of the accelerometer.

Translational accelerations

In the following we describe the procedure for deriving the equations of motion of one proof mass (A). The extension to a second proof mass is straight forward [v]. The CM vector in each body's reference frame is:

Body A: $\{r_A\} = \{x_{CMA}\ \ y_{CMA}\ \ z_{CMA}\}^T$

Body C: $\{r_C\} = \{x_{CMC}\ \ y_{CMC}\ \ z_{CMC}\}^T$

The translational acceleration expressed in the inertial reference is obtained by using the formula:

$$\{a_A\} = \left[\ddot{R}_{A0}\right]\cdot\{r_A\} + 2\left[\dot{R}_{A0}\right]\cdot\{\dot{r}_A\} + \left[R_{A0}\right]\cdot\{\ddot{r}_A\} + \left\{\ddot{R}_A^0\right\} \tag{7}$$

where $\{a_A\}$ is the acceleration of body A in the inertial frame, $[R_{A0}]$ is the rotation matrix from A to inertial frame, $\{r_A\}$ is the coordinates vector of body A CM in the A frame, $\{R_A^0\}$ is the translation vector expressed in inertial coordinates, and $(\cdot)$ indicates matrix multiplication. Same-structure equations are used for the additional bodies.

Elastic Forces

To evaluate the elastic forces we define first the points where the springs are attached to each body. The position of these points are expressed in body frame. The distance between connected points is then computed from the actual position during the motion, projected in the A frame, and multiplied by the stiffness vector $\{k_{xA},\ k_{yA},\ k_{zA}\}$. By following this procedure, it is possible to assign different stiffness to each degree of freedom. The elastic forces are then projected in the inertial coordinate system as follows

$$\{F_{1A}\} = [R_{A0}] \,.\, ([K] \,.\, (\{p_{A1}\} - [T_{0A}].\{T_{C0}.p_{C1}\} - \{l_1\}))$$

$$\{F_{2A}\} = [R_{A0}] \,.\, ([K] \,.\, (\{p_{A2}\} - [T_{0A}].\{T_{C0}.p_{C2}\} - \{l_2\})) \tag{8}$$

$$\{F_A\} = \{F_{1A}\} + \{F_{2A}\}$$

where $[K]$ is the spring stiffness matrix, $\{p_A\}$ and $\{p_C\}$ are the vectors that define the positions of the spring attachment points, and $\{l_1\}$ and $\{l_2\}$ are the natural lengths of the springs. The operator "$T_{0A}.x$" indicates the combination of a multiplication by the rotation matrix $[R_{0A}]$ applied to the vector $\{x\}$ plus the translation of the vector $\{R_A^A\}$ which yields:

$$\{T_{0A}.x\} = [R_{0A}].\{x\} + \{R_A^A\}$$

The expression $T_{0A}.(T_{C0}.p_{C1})$ projects the coordinates of the point p_{C1} (expressed in the body C frame) onto the body A coordinate system. Subsequently, the force is projected onto the inertial frame using the $[R_{A0}]$ matrix. A similar procedure is used to evaluate the forces acting on any other body pairs.

The equations of translational motion for the two bodies A and C finally yield :

$$m_A\{a_A\} - \{F_A\} = 0$$

$$m_C\{a_C\} - \{F_C\} = 0 \tag{9}$$

where m_A and m_C are the masses of body A and C, a_A and a_C the accelerations, and F_A and F_C the elastic forces:

$$\{F_A\} = \{F_{1A}\} + \{F_{2A}\}$$

$$\{F_C\} = \{F_{1C}\} + \{F_{2C}\}$$

The subscripts 1 and 2 identify the two springs that connect body A to C.

Rotational accelerations:

The angular velocity of each body is computed by using the rotation matrices that transform the coordinate system from the inertial to the body frame and, conversely, through the opposite transformation. The rotational velocity matrices of bodies A and C are derived by using the Cartan's formula as follows:

$$\begin{aligned} [\Omega_A] &= [R_{0A}] \cdot [\dot{R}_{A0}] \\ [\Omega_C] &= [R_{0C}] \cdot [\dot{R}_{C0}] \end{aligned} \qquad (10)$$

where $[R_{0A}]$ and $[R_{A0}]$ are the rotation matrices from the inertial coordinate system (denoted by 0) to the body reference frame of A and vice-versa. $[R_{0C}]$ and $[R_{C0}]$ are the correspondent matrices for body C. It should be noted that the former expression lead to the skew symmetric matrix of the angular velocity from which the components of the angular velocity vector $\{\Omega_A\}$ can be readily extracted.

Elastic torques

The elastic torques acting on each body are computed by using the expressions for the locations of the attachment points and elastic forces previously defined. The expressions of the torques in the respective body reference frames are as follows:

$$\begin{aligned} \{T_A\} &= \{p_{A1}\} \times ([R_{0A}] \cdot \{F_{1A}\}) + \{p_{A2}\} \times ([R_{0A}] \cdot \{F_{2A}\}) \\ \{T_C\} &= \{p_{C1}\} \times ([R_{0C}] \cdot \{F_{1C}\}) + \{p_{C2}\} \times ([R_{0C}] \cdot \{F_{2C}\}) \end{aligned} \qquad (11)$$

where $\times$ indicates the external product of vectors.

Invoking Euler's equations, the rotational equations of motion yield:

$$\begin{aligned} [I_A] \cdot \{\dot{\Omega}_A\} + [\Omega_A] \cdot [I_A] \cdot \{\Omega_A\} - \{T_A\} &= 0 \\ [I_C] \cdot \{\dot{\Omega}_C\} + [\Omega_C] \cdot [I_C] \cdot \{\Omega_C\} - \{T_C\} &= 0 \end{aligned} \qquad (12)$$

where $\{\Omega_A\}$ and $[\Omega_C]$ represent the angular velocity vector and matrix, respectively, for body A (and similarly for body C). $[I_A]$ and $[I_C]$ are the inertia matrices for body A and C which, assuming principal axes, have diagonal forms. The equations of motion for the complete three-body detector are evaluated in the same way as for the two-body example

used previously leading to 3 vector equations for the rotational dynamics and 3 equations for the translational dynamics.

Numerical cases

Figure 8 shows the configuration of the 3-body sensor utilized for the numerical cases and the positions of the attachment points for the three-body sensor.

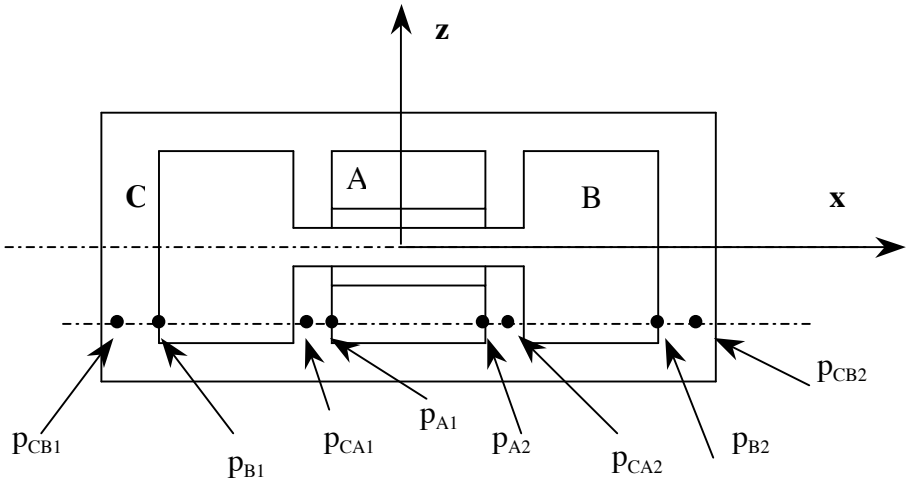

Figure 8 Attachment points of the proof masses

The points p_{CA1}, p_{CA2}, p_{CB1} and p_{CB2} are the points of the external body C connected to the points p_{A1}, p_{A2}, p_{B1}, p_{B2}, respectively. In this detector configuration, four springs are used to connect the two bodies to the external case (i.e., two springs per proof mass). The numerical value adopted for the numerical case shown in the following are as follows:

$m_A = 1$ kg, $m_B = 1$ kg, $m_C = 30$ kg;
$I_{Ax} = I_{Ay} = I_{Az} = 0.17$ kg-m^2; $I_{Bx} = I_{By} = I_{Bz} = 0.17$ kg-m^2;
$I_{Cx} = 0.95$ kg-m^2, $I_{Cy} = I_{Cz} = 1.46$ kg-m^2;
$k_{A1x} = 45000$ N/m, $k_{A1y} = k_{A1z} = 35000$ N/m;
$k_{A2x} = 45000$ N/m, $k_{A2y} = k_{A2z} = 35000$ N/m;
$k_{A\theta x} = 61.68$ Nm/rad, $k_{A\theta y} = k_{A\theta z} = 1000$ Nm/rad;
$k_{B1x} = 45000$ N/m, $k_{B1y} = k_{B1z} = 35000$ N/m;
$k_{B2x} = 45000$ N/m, $k_{B2y} = k_{B2z} = 35000$ N/m;
$k_{B\theta x} = 61.68$ Nm/rad, $k_{B\theta y} = k_{B\theta z} = 1000$ Nm/rad.

The initial conditions at release are: spin rate $\Omega_x = 1.885$ rad/s (0.3 Hz), angular error at release $\theta_y = 10^{-2}$ rad/s; and initial nutation angle = 0. The CM offset errors are (with the reference frame placed at the geometrical center of body C):

$x_{CMA} = 10^{-6}$ m, $y_{CMA} = 0$, $z_{CMA} = 10^{-6}$ m;
$x_{CMB} = 0$, $y_{CMB} = 0$, $z_{CMB} = 0$;
$x_{CMC} = 0$, $y_{CMC} = 0$, $z_{CMC} = 0$

From the point of view of the rigid-body dynamics, a detector with the above inertia characteristics is a minor-inertia-axis spinner that exhibits a prograde precession.

The natural elastic frequency of the detector are shown in Figure 9. The lowest frequency (at 2.999 Hz) corresponds to the differential torsional mode of the proof masses while the next one (at 3.486 Hz) corresponds to the common-mode torsional frequency.

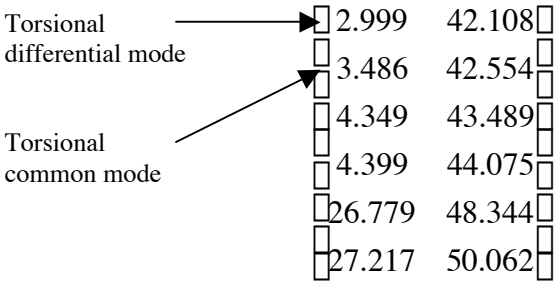

Figure 9 Natural frequencies

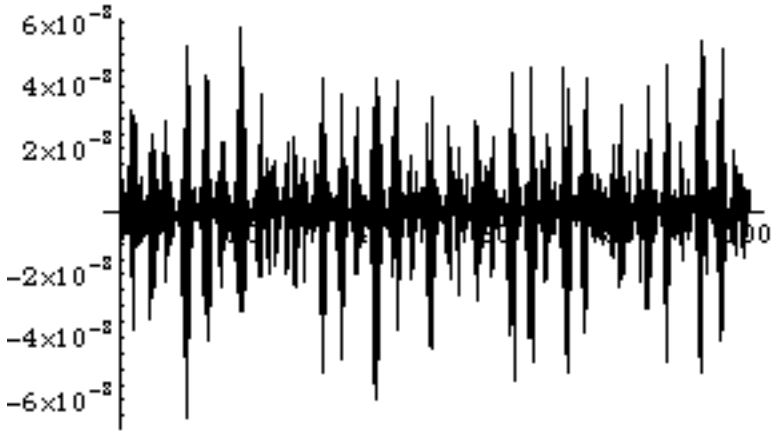

Figure 10 $y_A - y_B$ (m) in body frame vs. time (s)

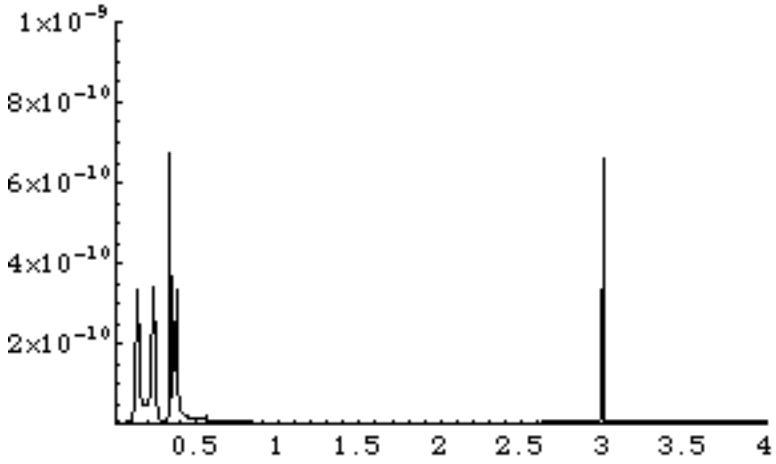

Figure 11 FFT of y_A - y_B (m) vs. frequency (Hz)

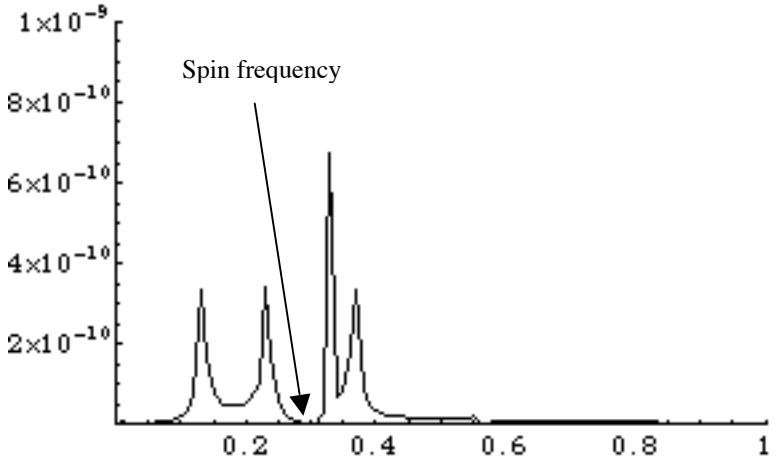

Figure 12 Zoom of y_A - y_B (m) FFT vs. frequency (Hz)

Figure 10 is a time profile of the differential displacement between the two proof masses, that is measured by the capacitive pickups. The displacement is then converted into acceleration through the accelerometer's transfer function. The initial conditions adopted for release are conservatively large and no post-release phase with oscillation damping was included in this simulation leading to conservative values of the differential displacements. Here we are mostly concerned with the frequency content of the differential displacement which is shown in Fig. 11 and, with an expanded view, in Fig. 12. Figure 11 shows the separation between the oscillations related to the rigid-body dynamics of the instrument package (at low frequency) and the first elastic frequency of the accelerometer. More importantly, Fig. 12 shows that the precession frequency can be chosen so that the harmonics related to the rigid-body dynamics do not overlap with the spin frequency (which is also the signal frequency).

The precession of the instrument package will be caused by an angular rate error (perpendicular to the spin axis) at release or an imperfect inertial balancing of the instrument package. Effects of the precession are detected by the accelerometer if the centers of mass of the proof masses do not coincide with the center of mass of the instrument package. If we choose the moments of inertia of the instrument package so that the precession frequency is non-commensurate with the spin frequency, then there are no dynamics-related harmonics at the signal frequency. Consequently, we must simply guarantee that the precession-related accelerations are smaller than the end-of scale of the detector. These conditions are met for a prograde precession (minor-axis spinner), angular rate errors at release smaller than about 0.1 deg/s, and realistic construction accuracies of the detector.

Conclusions

Our analysis concludes that the gravitational perturbations, acting on the test masses and due to the capsule gravity, can be reduced to within the limit required by the experiment if the test mass design abides to simple rules as follows:

a) The test masses must be smaller than a characteristic size of about 10 cm;
b) The second order principal moments of inertia must be equal within construction tolerances ($\Delta L/L < 10^{-4}$);
c) The density uniformity of the test mass must be within 0.01% ($\Delta M/M < 10^{-4}$).

There is no need for belted cylinders (used in the STEP satellite experiment) for the accuracy goal of our experiment.

With reference to the detector free-fall dynamics, the ratio of the moments of inertia of the instrument package must be such that the body precession frequency is non-commensurate with the spin frequency. Similarly, none of the elastic frequencies of the detector must overlap with the spin frequency. These conditions guarantee that no acceleration components related to the detector elastic and rigid-body dynamics overlap with the signal frequency.

Acknowledgements

This work was supported by NASA grant NAG8-1780 with Donald Strayer at the Jet Propulsion laboratory as Project Scientist and Dorthy Hubbard at NASA Marshall Space Flight Center as Technical Officer.

References

[i] Baessler, S., B. Heckel , E. Adelberger, J. Gundlack , U. Schmidt and E. Swanson, *Phys Rev Lett.,* Vol. 83, 1 Nov. 1999.

[ii] Williams, J.G., X.X. Newhall and J.O. Dickey (1996), Relativity parameters determined from lunar laser ranging, *Phys. Rev. D*, 53, 6730.

[iii] Lorenzini, E.C., I.I. Shapiro, F. Fuligni, V. Iafolla, M.L. Cosmo, M.D. Grossi, P.N. Cheimets and J.B. Zielinski, "Test of the Weak-Equivalence Principle in an Einstein Elevator." Il Nuovo Cimento, Vol. 109B, No. 11, 1994.

[iv] Lockerbie, N.A., A.V. Veryaskin and X. Xu, "Differential gravitational coupling between cylindrically-symmetric, concentric test masse and arbitrary gravitational source: relevance to the STEP experiment." Classic and Quantum Gravity, Vol. 10, 2419-2430, 1993.

[v] Shapiro, I.I., et al. "Test of the Equivalence Principle in an Einstein Elevator." Annual Report#2, NASA Grant NAG8-1780, June 2003.